CHAPTER 1
Introduction and Literature Review

CHAPTER 1.

Introduction and Literature Review

1.1 Introduction

Electroceramics spanning, both polar and non-polar dielectric materials are counted as high-demanding materials. The electronic parts made from electroceramics are used in various industries, including defense, medical, automobiles and telecommunications [1]. The majority of these electroceramics belong to the polar dielectric class that shows piezoelectricity, pyroelectricity and ferroelectricity. These are widely used in actuators, capacitors, sensors, motors and transducers. The piezoelectric device market is one of the fastest growing market and it is expected to grow from its present worth of 30.8 million USD to 41 million USD in 2027 [2]. The uses of piezoelectric materials are not only limited to the traditional industries relying on energy consumption, storage and conversion applications, but also are widely becoming popular in energy harvesters supporting sustainable development and in newly developing industrial fields from micro-robotics to bullets that can change direction [3].

The piezoelectric energy harvesters are used to capture energy that otherwise could be wasted in the form of wind, heat and mechanical vibrations generated from heavy machines, concrete constructions, etc., and convert it into electrical energy. The surplus waste energies, such, huge vibrational energies produced on the bridges from passing vehicles, heat observed around the engines that deliver high power, the work from human walking and exercising, etc. can be stored and used to power other devices using piezoelectric energy harvester coupled batteries, supercapacitors, generators, etc. [4]

The ability of piezoelectric ceramic materials to be used in multifunctional devices essentially relies on their ferroelectric (dipolar polarization orientation), electromechanical (d_{33} and k_{33}) and dielectric (dielectric constant, loss and electrical parameters) properties. A good combination of these properties is obtained in $Pb(Zr_xTi_{1-x})O_3$ (PZT) from the family of perovskite structured ceramics. It is the most commonly used piezoelectric ceramic materials [5,6]. The PZT is widely popular for its ultrasonic generator properties, quick response time, chemically inert behaviour and tunable electrical properties upon appropriate doping/additives. Commercial uses of PZT involve a wide range of applications, such as infrared sensors and transmitters, pyroelectric detectors, resonators, optical field effect transistors, lamb wave modulators and many more [7].

Among various forms and classes from which piezoelectric materials are selected for devices, viz., single crystalline, polycrystalline, polymers, composites, etc., the piezoelectric polycrystalline ceramics, also called as piezoceramics, cover the largest portion commercially. Piezoceramics are basically ferroelectric materials with polycrystalline structures. After proper poling, ferroelectric ceramics can act as piezoelectric materials [5]. The ability of ferroelectric materials to show spontaneous polarization with polarization direction switching in the presence of an externally applied electric field translates into the coupling of dimensional extension by displacement of ions producing electric charges by a very short length scale. The piezoelectric, dielectric and ferroelectric properties of piezoceramics deals with a combined effect of intrinsic (single-unit cell polarization) and macroscopic response. The macroscopic aspects are primarily concerned with the orientations and size of domains, size of grains and leakage currents etc., whereas the intrinsic polarization is

affected by the characteristics of individual ions, hybridization, close packing, crystal structure etc.

The Pb-based piezoelectric materials, especially PZT and $(1-x)Pb(Mg_{1/3}Nb_{2/3})O_3-xPbTiO_3$ (PMN-xPT) have been found to possess excellence in both intrinsic polarization as well as macroscopic response. Due to presence of Pb- in these compounds, the hybridization of $Pb-6s^2$ lone pair increases its contribution to ferroelectricity, at the same time, offers other merits such as the ready formation of larger domains, low coercive field giving the easy orientation of domains, high densification and low dielectric losses in bulk form making them highly desirable for several kinds of piezoelectric applications. The properties and utility of these materials also greatly relies on their crystal structure and composition. The optimal compositions of these solid solutions near the morphotropic phase boundary (MPB) region may exhibit maximized dielectric, ferroelectric and piezoelectric properties. The MPB region is defined as a nearly vertical phase boundary in the temperature-composition phase diagram of ferroelectric materials where two or more crystallographic phases coexist and crystallographic phase transitions occur. While having so many merits, the PZT and PMN-xPT still exhibit some drawbacks, viz., brittleness, fatigue and toxicity due to presence of Pb. Especially, the toxicity, being a serious concern to the environment and human in contact, researchers worldwide are working for discovering new lead-free piezoelectric alternatives. The subject matter of the present thesis is focused on the development of a new solid solution with lower Pb-concentrations and explore its crystal structure and properties as a function of composition and temperature. We have selected $(1-x)Ba(Cu_{1/3}Nb_{2/3})O_3-(x)PbTiO_3$ solid solution which is sparsely explored solid solution system.

Before discussing the results of our investigation on various compositions of (1-x)Ba(Cu$_{1/3}$Nb$_{2/3}$)O$_3$-(x)PbTiO$_3$ ceramic, a brief overview of basic terms and concepts required to understand the subject matter is given in forthcoming sections. This is followed by brief review of the existing literature and current status of research on the selected topic. At the end of this chapter, the main objectives of the present thesis are listed.

1.2   Piezoelectricity

The discovery of the piezoelectric effect in Quartz, Topaz and Rochelle salts by the Curie brothers Pierre and Jacques dates back to 1880. The word piezoelectricity translates as "pressure electricity" and is the observation of electric charge with an application of stress. More precisely, a direct piezoelectric effect is defined as an application of stress resulting in strained crystal, thereby developing non-centrosymmetric charge distribution leading to a net macroscopic electrical polarization. The indirect piezoelectric effect is known as its converse effect, i.e., application of an electric field produces strain in a piezoelectric crystal [7]. The thermodynamic potential generalizing electric field and mechanical stress in a piezoelectric media can be written as equation (1.1)

$$\varphi = \varphi_0 - \frac{1}{2}s_{iklm}T_{ik}T_{lm} - \frac{1}{2}\varepsilon_{ik}E_iE_k - E_iD_{i0} - d_{ikl}E_iT_{kl} \qquad (1.1)$$

Here, s_{iklm} is elastic compliance tensor, ε_{ik} is dielectric permittivity tensor, d_{ikl} is piezoelectric strain tensor, D_{i0} is related to spontaneous polarization, T is strain tensor, and E is electric field. The dielectric displacement vector component (D_i) and deformation stress component (S_{ik}) found by differentiating equation (1.1) are defined below in equations (1.2) and (1.3).

4

$$D_i = -\left(\frac{\partial \varphi}{\partial E_i}\right)_T = D_{i0} + \varepsilon_{ik}E_k + d_{ikl}T_{kl} \tag{1.2}$$

$$S_{ik} = -\left(\frac{\partial \varphi}{\partial T_{ik}}\right)_E = s_{iklm}T_{lm} + d^*_{ikl}E_l \tag{1.3}$$

Equation (1.2) contemplates the direct piezoelectric effect, and d_{ikl} is the direct piezoelectric strain coefficient. Similarly, equation (1.3) reflects the inverse piezoelectric effect, and d^*_{ikl} is the indirect piezoelectric strain coefficient. The non-centrosymmetric deformation of crystal for exhibiting piezoelectricity is allowed only in some particular classes of point groups in crystal symmetry [8]. Fig 1.1 is a pictorial representation of the categorization of these point groups. Applying crystal symmetry restriction and using suitable concise notation, the piezoelectric tensor is reduced to fewer independent piezoelectric coefficient components. A detailed description can be found elsewhere [9]. For piezoceramics to exhibit piezoelectricity, they need to be ferroelectric, that is allowed only in a few point group symmetries, as listed in Table 1.1 with the crystal structure.
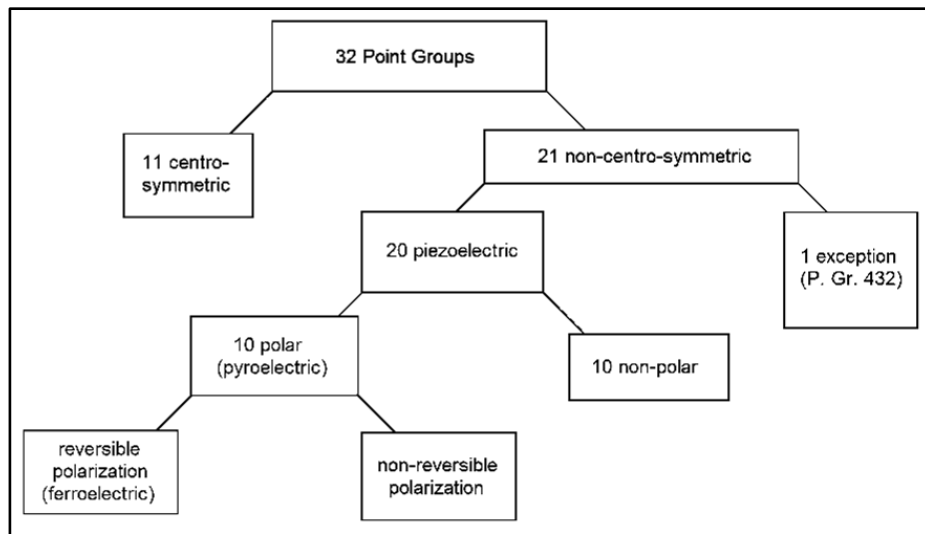

Fig 1.1 Illustration of dielectric crystal classes and their subdivision [adopted from [8]]

Table 1.1 Point groups in pyroelectric crystal class

Crystal System	Point Group
Triclinic	1
Monoclinic	2, *m*
Orthorhombic	*mm*2
Rhombohedral	3, 3*m*
Tetragonal	4, 4*mm*
Hexagonal	6, 6*mm*

1.3 Ferroelectricity

Ferroelectricity is defined as the state of materials in which it is spontaneously polarized, even in the absence of an external electric field, and polarization is reversible under externally applied electric field. The ferroelectric property depends upon the non-centrosymmetric crystallographic arrangement of ions in the materials; in other words, the polarization originates through a decrease in the crystal symmetry. All ferroelectric materials do not always exhibit ferroelectricity, but it depends on certain conditions. For example, ferroelectricity can be exhibited only below a specific Curie temperature, above which a centrosymmetric paraelectric state is observed in ferroelectrics. Additionally, a single-crystalline material does show ferroelectric behaviour below its curie temperature, whereas in polycrystalline ceramics, the ferroelectric domains may exist in a random orientation, giving a net zero polarization. In such a case, the ferroelectricity is observed by aligning domains with the aid of a high electric field. The applications of ferroelectric materials are enormous in the area of electronics,

automotive industries, as dielectrics for capacitors, healthcare and defense sectors. They are most widely used as piezoelectric ceramics in various devices such as shock wave generators, ultrasonic imaging devices, transformers, high-power transducers, piezoelectric buzzer devices, printers, ignition devices, etc. Understanding the phenomenon of phase transitions in ferroelectric materials is key to grasp the origin of ferroelectricity in these materials [8].

1.4 Landau Theory of Phase Transitions

The polarization vector P is regarded as an order parameter in Landau's theoretical explanation of ferroelectric phase transitions and it is accountable for the symmetry deviations of the crystal structure [1,9]. The free energy (G) expansion in terms of polarization vector for a unique ferroelectric axis can be written as given in equation (1.4).

$$G = -EP + G_0 + \frac{1}{2}G_2 P^2 + \frac{1}{4}G_4 P^4 + \frac{1}{6}G_6 P^6 + \cdots \qquad (1.1)$$

Here, G_0, G_1, … G_n are the temperature-dependent coefficients. The odd powers of P is not taken in the free energy density expansion since in the cubic-paraelectric phases its inversion will change sign and it must be invariant with respect to polarization reversal in paraelectric phase. Therefore, only even terms are taken into account in this expansion [4]. The derivatives of the free energy give crucial parameters associated to different stable phases. The first order derivative gives the values of spontaneous polarization for observed minima, and the second order derivative gives the susceptibility (χ^{-1}) and correspond to Curie-Weiss law. Depending on different values of G_n, the different states of the ferroelectric materials are observed [9]. An absolute

minimum is obtained for free energy if temperature $T > T_c$ (paraelectric phase), while two minima are observed for $T < T_c$ (ferroelectric phase). The T_c is ferroelectric to paraelectric phase transition temperature. The typical first-order and second-order phase transitions of ferroelectric materials also reside on the values of G_n. The free energy profile for different cases of varying G_n is shown in Fig 1.2. Near tri-critical points in ferroelectric materials, a much flatter energy profile for polarization reversal is visible around T_c [9].
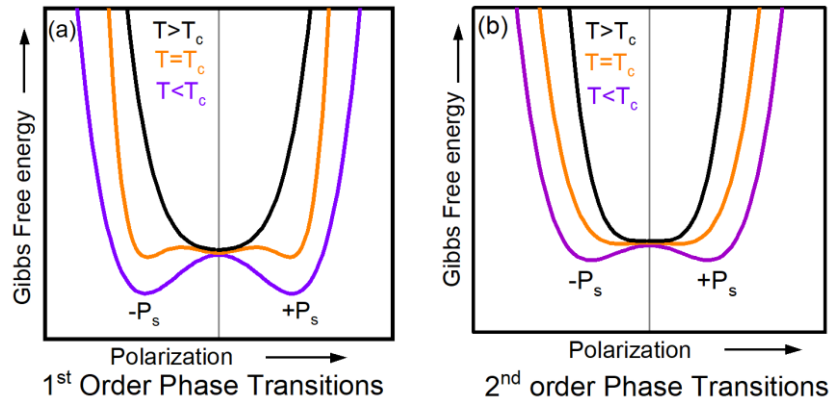
Fig 1.2 Evolution of Gibbs free energy in ferroelectric materials near T_c

In ferroelectric materials, the phase transitions between the ferroelectric states of different crystallographic symmetry containing phases, such as tetragonal, rhombohedral, orthorhombic, monoclinic etc., also needs the consideration of anisotropy of the polarization vector 'P', which is an order parameter in different crystallographic directions. For a stress-free crystal at a specific temperature, the anisotropic expansion of free energy expressions are given the equation (1.5).

$$G_{aniso}(P) \equiv G_{000} + G_{200}\left(p_x^2 + P_y^2 + P_z^2\right) + G_{400}\left(p_x^4 + P_y^4 + P_z^4\right)$$
$$+ G_{220}\left(p_x^2 p_y^2 + P_y^2 p_z^2 + P_z^2 p_x^2\right) + G_{600}\left(p_x^6 + P_y^6 + P_z^6\right) + \cdots$$

(1.5)

Just like the previous discussion, the evolution of these phases also depends upon the coefficient of expansion of anisotropic free energy. The minima of free energy for $P\|<100>$ direction results for the tetragonal phase while same for $P\|<111>$ due to the rhombohedral phase, considering the free energy expansion up to 2nd order. The other low symmetry phases, however, can only be observed if the expansion of free energy is considered up to higher terms, viz., 6th order for orthorhombic phases by observing 'G' minima in $P\|<110>$ direction [9], 8th order for monoclinic phases by observing 'G' minima in $P\|$ to planar direction instead of axial direction [10], and 12th order for triclinic phases [11]. The polarizing state or specific symmetry of a ferroelectric material in these crystallographic directions is finely governed by the lattice vibrations and evolution of different modes as a function of temperature or any other variable affecting the phase stability [4].

1.5 Soft Phonon Modes

The phase transitions in the ferroelectric materials are viewed as the dependencies over the stability of normal vibrational modes of the crystal lattice, called as soft phonon. When the temperature of a ferroelectric material is decreased to observe the ferroelectric state from paraelectric state, the polar soft phonon mode frequency decreases and becomes zero at T_c. The frozen mode displacement results into development of polarization vector which is then realized as the order parameter of the ferroelectric state [4].

1.6 Differentiation of Ferroelectrics from Antiferroelectrics and Relaxor Ferroelectrics

The *antiferroelectric* state comes into the picture when the soft phonon modes condense at the Brillouin zone boundary. This leads to the formation of two types of sub-lattices of polarization (P+ and P-), opposite to each other. In the absence of an electric field, the net microscopic polarization in antiferroelectric is zero and they show a typical double hysteresis loop. The thermodynamic potential of these sublattices is then considered as an independent thermodynamic variables, and the free energy can then be written as equation (1.6) [4].

$$G_{af}(T, P_+, P_-) = G_0(T) + G_\alpha(p_+^2 + P_-^2) + G_\beta(P_+P_-) + G_\gamma(p_+^4 + P_-^4) + \cdots \quad (1.6)$$

In contrast, the *Relaxor ferroelectrics* show a glass-like transition upon cooling instead of undergoing a typical phase transition. These materials exhibit broad freezing transitions of polarization vector that comes from nano-polar regions and display frequency-dependent maxima in temperature-dependent dielectric responses. When the cooling is imposed, the thermal fluctuations of the paraelectric phase play an important role. Below Burns temperature, nano polar region (NPR) forms in a relaxor material. At this state, a high density of domain walls is observed with a mixture of paraelectric and ferroelectric-like unit cells, accompanied by the phenomenon of polarization rotation. These NPRs interact with stress and produce softening of elastic modulus, leading to high electromechanical responses [4,12].
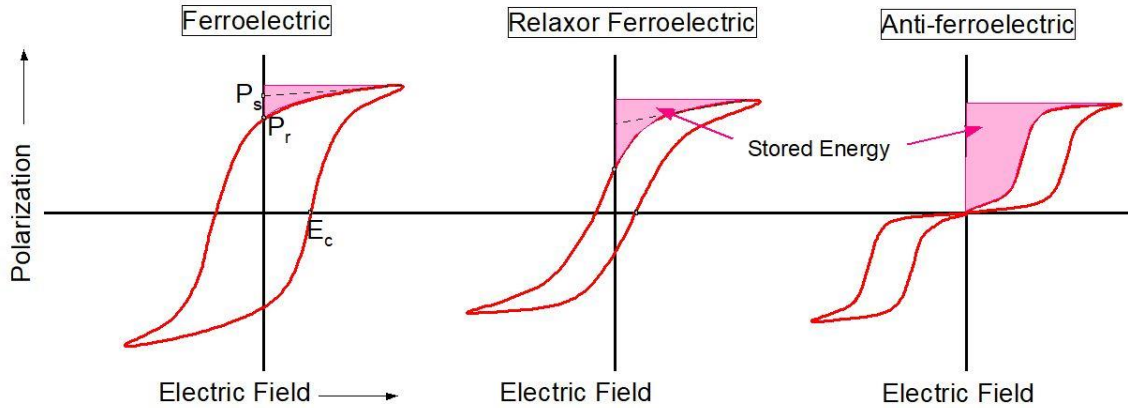
Fig 1.3 Schematic presentation of P-E loops and stored energy density in ferroelectric, relaxor ferroelectric and anti-ferroelectric materials

Fundamental differences between the ferroelectric, antiferroelectric, and relaxor ferroelectric materials can also be visualized in the behaviour of macroscopic polarization on the application of an external electric field. Fig 1.3 shows the ideal Polarization (P)-Electric field (E) loops exhibited by these materials. A ferroelectric material exhibits broad saturated hysteresis loop while a relaxor ferroelectric shows slim hysteresis loop with relatively much lower value of remnant polarization at zero field. In contrast, the Antiferroelectrics show characteristic double hysteresis loop due to presence of two independent polar sublattices. Integrating the electric field over polarization evaluates energy stored per unit volume in these materials. The useful energy is the recoverable energy subtracted from the corresponding hysteresis losses. Therefore, antiferroelectric materials are the best choice for energy density storing applications such as high-strain actuators, capacitors, pyroelectric detectors, pulsed voltage suppliers, etc.

Normal ferroelectric materials and relaxor ferroelectric can also be well distinguished on their temperature dependent behaviours of polarization, dielectric permittivity and inverse permittivity as illustrated in Fig 1.4. The normal ferroelectric

11

materials contain macro-sized ferroelectric domain which vanished above T_c, while in relaxor ferroelectric materials, the nano-sized domains persist well above their dynamic transition temperature (T_m). This distinct nature of domains in relaxors and normal ferroelectrics leads to different type of behaviour in dielectric permittivity as schematically shown in Fig 1.4. Sharp-narrow transitions are seen in normal ferroelectric materials, whereas the frequency-dispersive-broad transitions are observed for relaxors.
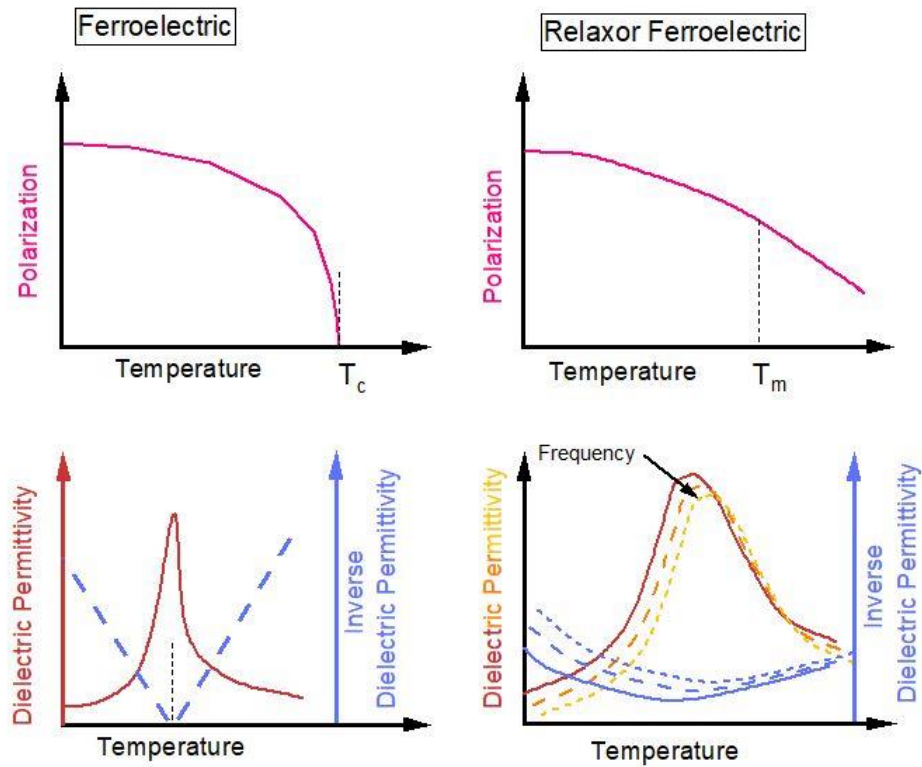
Fig 1.4 Temperature-dependent characteristics of normal ferroelectrics and relaxor ferroelectrics

1.7 Ferroelectric Perovskites

A large class of ferroelectric materials belongs from the perovskite structures. The ideal ABO_3 perovskite structure can be regarded as the cubic close-packed structure

of oxygen ions with B-site cation occupying central octahedral cage and A-site cations occupying dodecahedral sites, as shown in Fig 1.5. In the ABO_3 perovskite structure, the B-site cation inhabits a 6-fold, i.e., octahedral coordination, while the A-site cation inhabits a 12-fold, i.e., cuboctahedral coordination. At the primitive cubic unit cell level, the corners are occupied by the A-site cations, the body centre by B-site cations and the oxygen ions stacked as cubic close-packed layers along the cubic [111] direction [13]. The cubic crystal system exhibits *Pm-3m* space group in the ideal perovskite structure in which the A-site cation occupies (0, 0, 0) positions on the 1(a) Wyckoff site, B-site cation occupies (1/2, 1/2, 1/2) positions on the 1(b) Wyckoff site, and the O anions occupies (1/2, 1/2, 0) positions on the 3(c) Wyckoff site.
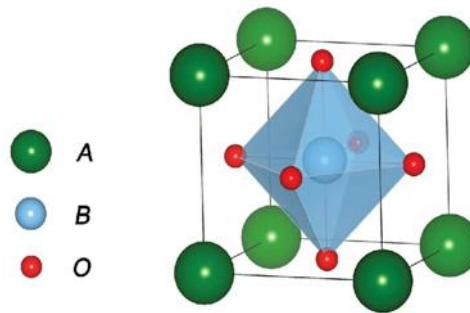
Fig 1.5 Schematic representation of ABO_3 perovskite structure

The A and B-sites can accommodate single or multiple cations with a total valeny of '+6' to preserve the charge neutrality, without disturbing the stability of perovskite structure, under certain conditions. The ***Goldschmidt tolerance factor*** (G_{tf}), defined in equation (1.7), is used to predict the possibility of formation of stable perovskite structure. Usually, the radial distance between A-site/B-site ions and oxygen is the sum of their ionic radii in their respective oxidation states; however, in the case of hybridization, the same gets shortened. A perfect fit of cations in the oxygen cavity

yields, $G_{tf} = 1$. For $G_{tf} \neq 1$, these values also indicate the possible stacking mode within the crystal. For example, when its value $G_{tf} > 1$, the close-packing is expected in <110> directions, while for $G_{tf} < 1$, the close-packing exists in <100> directions. In the former case, the A-site ions are tangent to oxygen ions, and the off-centering is allowed due to space in the B-O_6 octahedra, such as in $BaTiO_3$ and $KNbO_3$. In the latter case, B-site ions are tangent to oxygen ions, like in $GdScO_3$ [13] [14].

$$G_{tf} = \frac{r_{A-O}}{r_{B-O} * \sqrt{2}}$$ (1.7)

The perovskite-structured ferroelectric materials are capable of exhibiting many useful applicative features by tuning their compositional concentration due to the customizable crystal structures that accommodate ions with a broad range of ionic radii and valences without compromising the stability [13]. For example, in its ABO_3 type structure, the perovskite A-site cation can simultaneously have ionic radii as small as 1.17Å (Bi) to as big as 1.61Å (Pb), and valency variation from '+1' (Li, Na) to '+3' (Bi). Likewise, the perovskite B-site cations can also possess ions from 0.53Å (Mn^{+4}) to 0.77Å (Cu^{+1}) ionic radii along with a variation of '+1' (Cu^{+1}) to '+6' (W^{+6}) in valence states, demonstrating greater flexibility of the perovskite structure. Such a variety of sizes and valences in the structure have been seen to introduce fascinating phenomenon in the perovskite structured materials. For example, variable valency can be utilized to alter the conductivity of the materials, whereas large ionic radii differences can sometimes lead to ordering in the crystal structure [15,16].

In 2008, Cohen proposed that the ferroelectric nature of oxide perovskite can be predicted computationally by first principal calculations of the local approximations. The off-centering of the ions in the perovskite structure is a result of long-range and

short-range Columbic forces. This off-centering is directly related to the electric dipole moment of the materials and hence the polarization [14]. The short-range repulsive forces favouring the ideal cubic structure are compensated by the additional hybridization of the nd-orbital of the B-site cation and the 2p-orbital of oxygen ion. Moreover, in many cases, the presence of $6s^2$ lone pair of the Pb and Bi ions also supports the off-centering of the A-site ions. Pb-containing perovskite ceramics are the most important and widely used ferroelectric materials. Different chemical modifications can be made in them to obtain high piezoelectric and ferroelectric properties.

1.8   Morphotropic Phase Boundary

Although discouraged worldwide due to their toxicity, Pb-based perovskites dominate the piezoelectric industry owing to their excellent electromechanical properties, which come from the Pb-$6s^2$ lone pair and their hybridization with O-2p orbitals [17]. Many PbTiO$_3$ (PT)-based solid solutions having a perovskite-type structure also possess a morphotropic phase boundary (MPB), where maximized responses of dielectric, ferroelectric and piezoelectric properties are observed [5,18]. The MPB region is almost vertical in the composition versus temperature phase diagram of the solid solution, where two crystallographic phases may coexist, and on either side of the region beyond this boundary, only one of them is stable. The origin of high responses in physical properties in the MPB region is finely related to minute changes in the crystal structure of the materials while maintaining an appropriate balance of additional supplementary variables such as density, grain size, leakage current, etc. [19] These minute crystal structural variations are accompanied by a few other associated

15

phenomenon like the presence of NPR [20], softening of elastic modulus [21,22], presence of monoclinic phases [23,24], adaptive phases with nanodomains [10,25], thermodynamic phase instability [18], etc., leading to a flattening of the free energy landscape with enhanced ease of polarization switching/rotation under an externally applied electric field/stress [26].

1.9   Phase Diagrams

The phase diagram provides a prompt and simplified behaviour of materials for understanding and interpretation of their physical properties. With the precise location of MPB, one can predict the optimum compositions of the solid solution for which the maximum dielectric and piezoelectric properties will be obtained near these phase boundaries. Due to this, an insurgence in investigative studies has been observed in the last 50-60 years over determining the crystallographic structural states near MPBs, which eventually needs the complete construction of phase diagrams. The most commonly studies phase diagrams are of PZT, PMN-xPT materials and their phase diagrams have been extensively investigated using different experiments such as elastic x-ray and neutron scattering, Raman scattering, elastic modulus, IR spectroscopy, SAED and domain imaging by TEM, etc. [9,21]

A phase diagram of PZT drawn from the results of various experiments is shown in Fig 1.6. The figure was constructed by Cordero in 2015 [9] by combining the results of Jaffe et al. [5], Noheda et al [27], Rossetti et al. [10], Ragini et al. [28], and Singh et al. [21] mostly XRD studies, dielectric experiments of Cordero et al. [29], Buixaderas et al. [28], Ragini et al. [28], and Arlt [30], Raman experiments of Souza at al. [31], IR reflectivity analysis of Buixaderas et al. [28], elastic property experiments of Cordero et

al. [29], Ragini et al. [28] and Singh at al. [21] etc. The resulting crystallographic phases shown in Fig 1.6 are orthorhombic (O-antiferroelectric, *Pbam*) rhombohedral (R-high temp, *R3m*; R-low temp, *R3c*), tetragonal (T-ferroelectric, *P4mm*), cubic (C-paraelectric, *Pm-3m*) and monoclinic (M$_A$ and M$_B$-ferroelectric; *Cm,* M$_C$-ferroelectric, *Pm*).
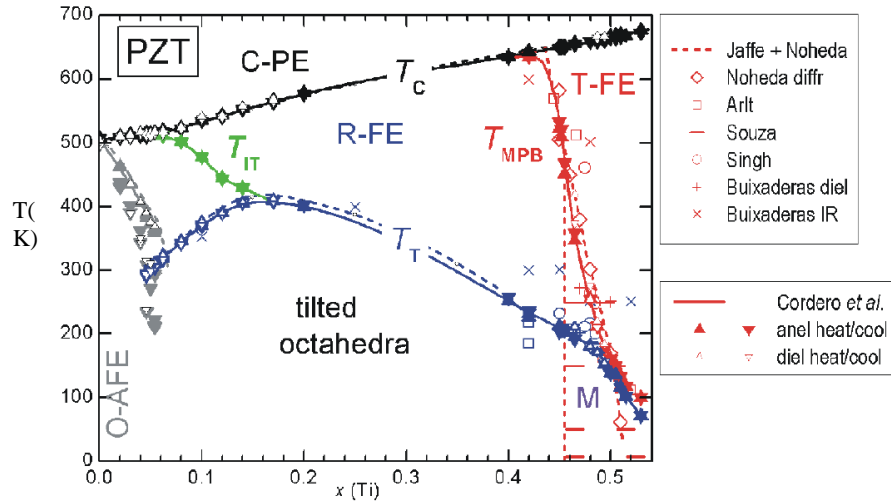

Fig 1.6 Phase diagram of PZT [adopted from [9]]

A 3D temperature-composition-electric field [001] phase diagram of PMN-xPT single crystal, constructed by I.H. Kim et al. [32], is shown in Fig 1.7. Similar to PZT, PMN-xPT also has been investigated by a number of researchers with sophisticated experiments and computational studies predictions. Some of the research groups working on revealing its crystal structure, from as early as 1990 to till date, are Shrout et al., B. Noheda et al., D. Cox et al., J. Shirane et al., D. Vanderbilt and M.H. Cohen, K. Uchino et al., D. Damjanovic et al., and A.K. Singh et al. [7,18,32–36]. The possible symmetry of this solid solution is very sensitive to different variables in MBP compositions and changes depending on temperature, concentration, crystallographic orientation and electric field. The demonstrated phase diagram in Fig 1.7 contains cubic,

rhombohedral, tetragonal, orthorhombic, monoclinic and triclinic phases for various compositions during the phase transitions occurring at different temperatures and electric field.
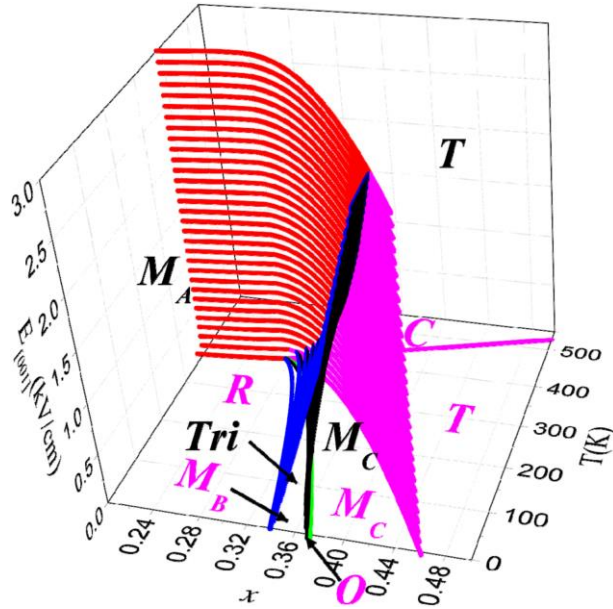

Fig 1.7 Temperature-composition-electric field phase diagram of PMN-xPT single crystal [adopted from [32]]

1.10 Monoclinic Phases, Polarization Rotation and Origin of Enhanced Piezoelectric Responses

The appearance of the intermediate monoclinic phases for the MPB compositions in the PZT and like solid solutions are described in various ways in the literature [18]. Its origin, existence, and contribution to high piezoelectric performances are often debated. In PZT, it is commonly accepted that the polarization vector rotates from the <100> direction in tetragonal phase to the <111> direction in rhombohedral phase via a stress-mediated deformation to accommodate the monoclinic phase. Fig 1.8 shows a schematic illustration of the direction of polarization in the three phases. An

increased number of favourable polarization directions, leading to a flat free energy landscape is believed to be the reason for its high performance in dielectric and elastic susceptibilities. A much more flattening of the free energy profile is also observed near tri-critical points.
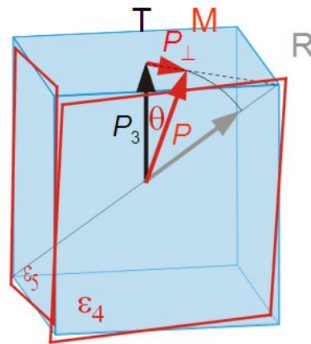

Fig 1.8 Schematic illustration of polarization rotation among tetragonal, monoclinic and rhombohedral phases [adopted from [18]]

Further, the stabilization of the monoclinic phase in compositions close to MPB can be induced by the electric field poling (see Fig 1.7), creating compositional disorders causing strong local distortions, applying pressure, or as a result of nano-twinning. The presence of a monoclinic phase, however, is not entirely sufficient for the high performance of piezoelectric responses; instead, they result from a high strain and large elastic compliance value, which are also capable of changing crystal structure from tetragonal and rhombohedral to monoclinic one.

1.11 Toxicity of Pb

Pb-based piezoelectric ceramics are the market leaders in the dielectric materials-based industries. They are widely used in various industries due to their excellent piezoelectric, dielectric, and ferroelectric properties [37]. When consumed directly or indirectly, the divalent nature of Lead can replace the calcium, magnesium

and sodium ions within the human body, which, thereby, reduces the affinity for essential enzymes for haemoglobin synthesis. The long-term exposure to low-level Pb poisoning can also result in neurological deficits. Other side effects of its exposure include symptoms of lethargy, vomiting, nausea, and abdominal pain. Some significant effects have also been found on various fundamental cellular processes like intracellular and intercellular signalling, cell adhesion, protein folding and maturation, apoptosis, ionic transportation, enzyme regulation, etc. Given such adverse effects of Pb and consequent worldwide restrictions on its uses, materials researchers have engaged to find its better alternatives [38,39].

1.12 Recent Development in MPB-based Solid Solutions and Defect-Engineered Materials

Exploration of the dielectric and piezoelectric properties of MPB compositions and their correlation with structure have been widely studied for popular ceramic materials such as PZT, PMN-xPT, etc. [12,40,41] Recently, Li et al. (2020) conducted a comparative study of rare-earth doped PMN-xPT ceramics by addressing their effects on the local structure and piezoelectric properties [40]. Extremely high piezoelectric response (d_{33} >1500pC/N) has been observed in 2.5% Sm-doped MPB composition of PMN-xPT in polycrystalline form as a result of increased "local structural heterogeneities" [40]. Fig 1.9 shows the piezoelectric coefficient, dielectric permittivity and field-dependent strain values for two MPB compositions of PMN-xPT reported by Li et al [40].

A recently discovered Pb-free Sn-doped $BaTiO_3$ (BT) possesses some of the highest piezoelectric responses in polycrystalline form, as reported by Wang et al. [42].

Various lead-free materials with good electromechanical properties and d_{33} responses suffer from drawbacks such as low Curie temperature (BT), hygroscopic nature [K(Na,Nb)O_3 (KNN)], low permittivity (LiNbO$_3$, Bi$_4$Ti$_3$O$_{12}$), low depolarization temperature and high coercive fields [(Bi,Na)TiO$_3$ (BNT)], high leakage current [BiFeO$_3$ (BFO)] [6,43,44]. Comparative responses of some of these materials along with a few PZT-based ceramics are shown in Fig 1.10(a). A maximum piezoelectric coefficient (d_{33} >1120pC/N) was observed for a critical compositional existence of multi phases (cubic-26%, tetragonal-25%, rhombohedral-17% and orthorhombic-3%) in the crystal structure.
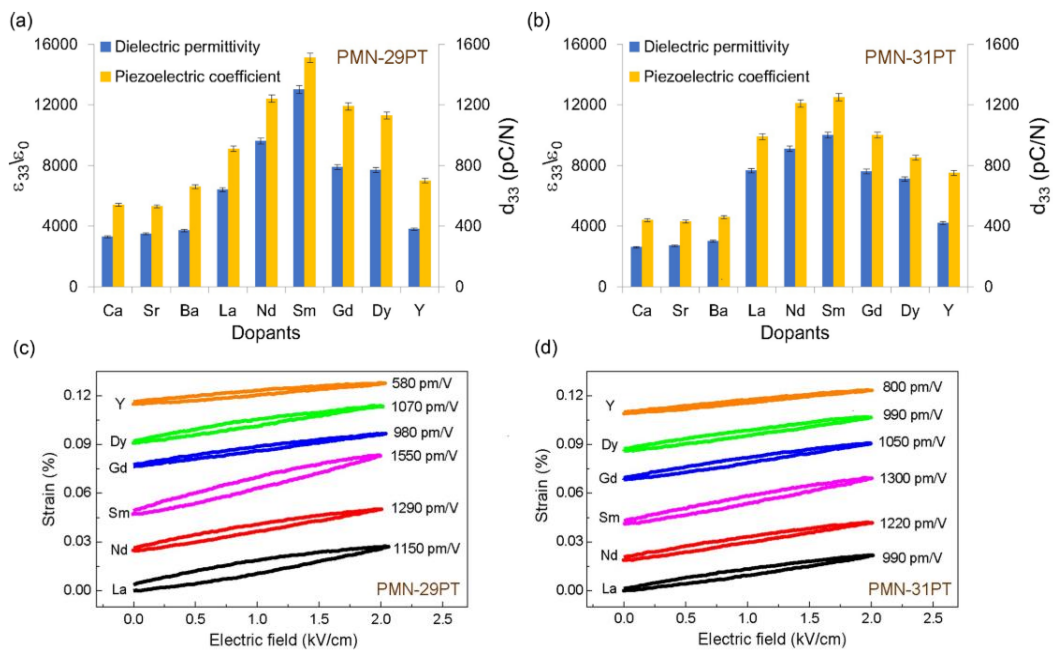
Fig 1.9 Room-temperature piezoelectric d_{33} coefficient and dielectric permittivity for 2.5 mol % Sm-doped (a) PMN-29PT and (b) PMN-31PT; electrical-field-induced strain curves for 2.5 mol % Sm-doped (c) PMN-29PT and (d) PMN-31PT [adopted from [40]]
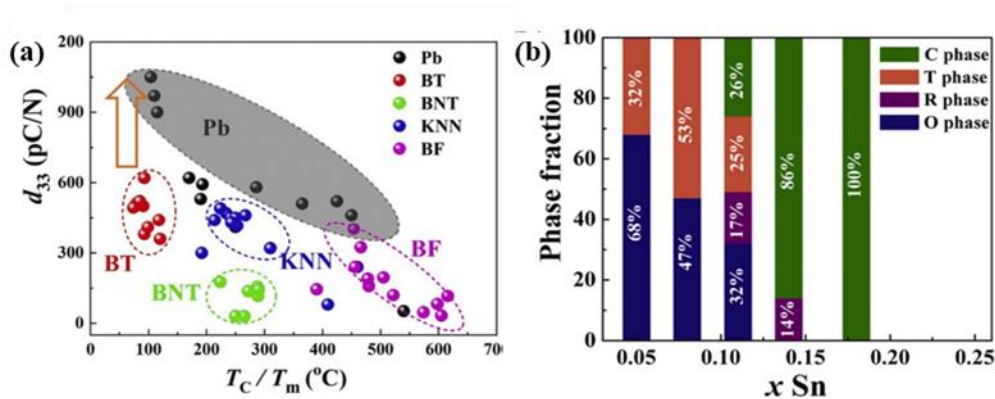
Fig 1.10 (a) A comparison of d_{33} vs. T_C/T_m for different piezoelectric ceramics, with the highest performance for 0.11% Sn doped BT highlighted with star symbol, (b) different phases in BT ceramic as a function of x mol% Sn. [adopted from [42]]

Numerous studies are being conducted to overcome the demerits of piezoelectric ceramics by doping, using additives and combining other materials to form their solid solution [6,37]. Apart from the inclusion of MPB into solid solution design, different approaches, like defect engineering, chemical substitutions/additives, textured grain orientations, etc., are among some promising ways to enhance the ferroelectric and piezoelectric characteristics of these materials. In defect engineering, the defects are created and controlled by introducing ions of different valency and sizes in both, stoichiometric and non-stoichiometric ways and/or creating cationic and anionic vacancies through heat treatment processes such as prolonged annealing and quenching [45]. Many dopants, such as oxides of Mn, Fe, Mg, La, Ce, Sb, etc., are well-known for inducing variation in the characteristics of perovskite materials. Especially the leakage current, which is undesirable in piezoelectric and ferroelectric properties but desirable in SOFC-like applications, can be tuned by the non-stoichiometric incorporation of these cations. A few additives, such as CuO, MnO_2, SiO_2, Co_3O_4, Fe_2O_3, MgO, Sb_2O_5 etc., are also have been reported for improving ferroelectric and piezoelectric properties by increasing resistivity and reducing losses in many ferroelectric ceramics [46][47]. The

additive also enhances various dielectric and piezoelectric properties and density of ceramics as illustrated in Fig 1.11 and Fig 1.12. By adding these additives usually stoichiometry of the material is tailored and subsequent hardening and softening effect are observed, which deals with the stabilization and ease of rotation of polarization for applied electric field, respectively. The Nguyen et al. (2021), defined three models for explaining hardening effect in lossy dielectric materials, viz., bulk effect, domain-wall effect, and grain boundary effect [48]. In these effects, different mechanisms of pinching of the domains due to defects have been explained.
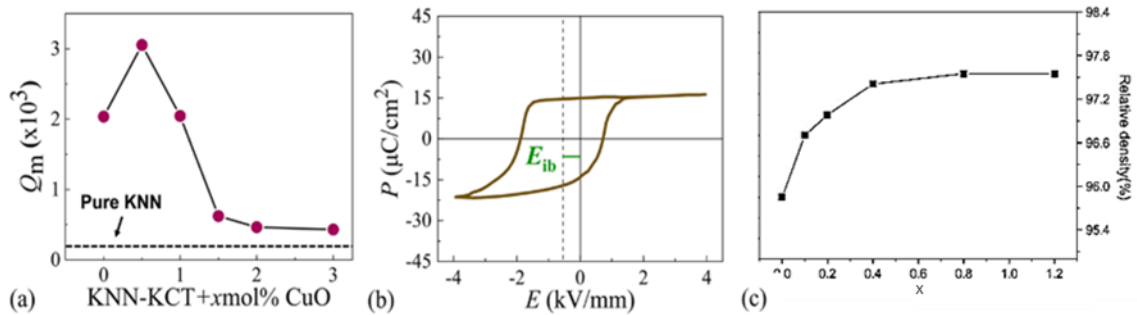
Fig 1.11 Tailoring of the physical properties in KNN-modified ceramics. Variations of (a) Mechanical quality factor of x mol% CuO doped $(K_{0.5}Na_{0.5})NbO_3-K_{5.4}Cu_{1.3}Ta_{10}O_{29}$, (b) P-E loop of 0.5 mol% CuO doped $(K_{0.5}Na_{0.5})NbO_3-K_{5.4}Cu_{1.3}Ta_{10}O_{29}$ and (c) sintering density for x mol% MnO_2 modified $(K_{0.5}Na_{0.5})_{0.94}Li_{0.06}NbO_3$ [adopted from [48,49]]
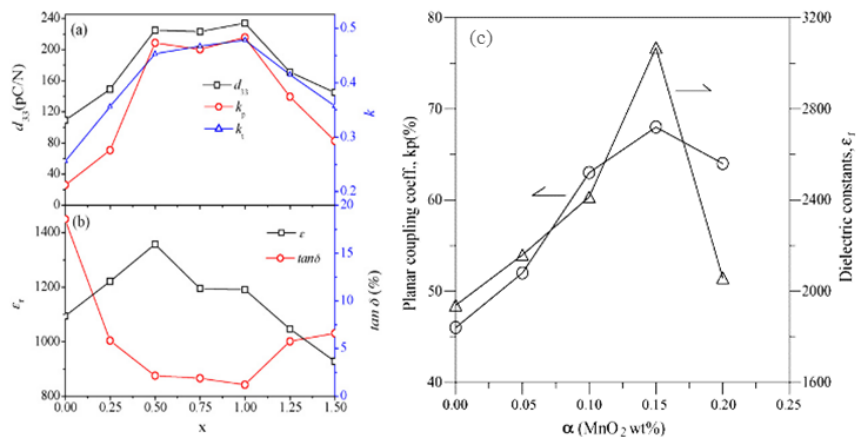

Fig 1.12 MnO_2 modified piezoelectric and dielectric property enhancement. (a) Variation of d_{33}, k_p, and k_t, (b) ε_r and $tan\delta$ in x mol% added $0.94(K_{0.5}Na_{0.5})NbO_3-0.06Ba(Zr_{0.05}Ti_{0.95})O_3$ ceramics (c) k_p and ε_r of α wt.% MnO_2 in $0.12Pb(Ni_{1/3}Sb_{2/3})O_3-0.48PbTiO_3-0.40PbZrO_3$ ceramic [adopted from [50,51]]

23

The effect of hardening can be seen in the form of asymmetry of the P-E hysteresis loop in Fig 1.12(b) for 0.5 mol% CuO doped $(K_{0.5}Na_{0.5})NbO_3$-$K_{5.4}Cu_{1.3}Ta_{10}O_{29}$ ceramic. The effect of different additive in modified KNN is shown in Fig 1.11 for increment in (a) mechanical quality factor (Q_m) of x mol% CuO doped $(K_{0.5}Na_{0.5})NbO_3$-$K_{5.4}Cu_{1.3}Ta_{10}O_{29}$ and (c) sintering density for x mol% MnO_2 modified $(K_{0.5}Na_{0.5})_{0.94}Li_{0.06}NbO_3$. The involvement of different doping and additives create reduction in leakage current by engaging the point charged effect into dipolar defects [48,52]. The effect of MnO_2 additive have been shown in Fig 1.12 in modified PZT and KNN ceramics.

1.13 Preliminary Studies on Ba(Cu$_{1/3}$Nb$_{2/3}$)O$_3$ and its Solid Solution

An early mention of the Ba(Cu$_{1/3}$Nb$_{2/3}$)O$_3$ (BCN) compound was made nearly 56 years ago by Kapyshev et al. [53]. An attempt of its synthesis in almost pure perovskite phase was performed by Langbein et al. in 1997 using both the solid-state reaction method as well as thermal decomposition of freeze-dried oxalate precursors, but the XRD peaks did not result well resolved XRD peaks after calcination [54]. Later on, a detailed investigation of the crystal structure and other physical properties such as microstructural, dielectric and magnetic properties of the compound was carried out in the 21st century by Priya et al. [47,55] and Zhang et al. [56] and the results are illustrated in Fig 1.13(b-h). Although the authors (Priya et al. [55]) could not get the pure phase in the calcined sample, they did observe the pure phase at a high sintering temperature of 1200°C as shown in Fig 1.13(a$_2$). The BCN compound is reported to be ferroelectric with a high Curie temperature of around 520°C, as confirmed by dielectric measurements and high-temperature XRD studies shown in Fig 1.13(a$_1$ and b) [47,56].

An observation of ferroelastic lamellar domains having planar nanodomain walls of thickness ~10-20 nm crossed at an angle of ~90° was also done by M. Song et el. [55] in the bright field TEM images of BCN pellets, as shown in Fig 1.14. They recorded images at different magnifications along with their SAED pattern to find out any ordering in the compound.
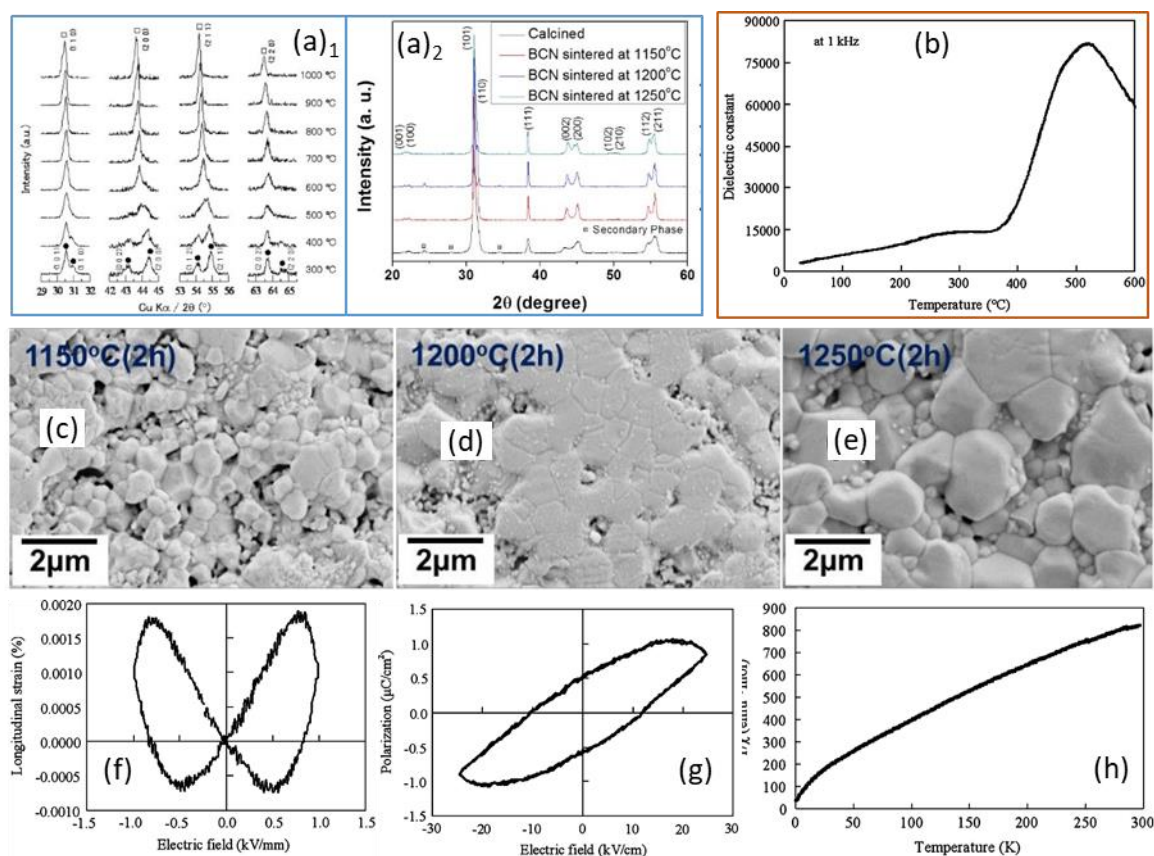

Fig 1.13 Various physical properties of BCN; (a_1) temperature-dependent XRD patterns of selected Braggs' reflections; (a_2) XRD pattern at different calcination and sintered conditions; (b) relative dielectric permittivity as function of temperature; (c, d and e) SEM micrographs of BCN sintered at 1150°C, 1200°C and 1250°C, respectively; (f) S-E loop; (g) P-E loop and (h) temperature-dependent inverse magnetic susceptibility [adopted from [47,55,56]]
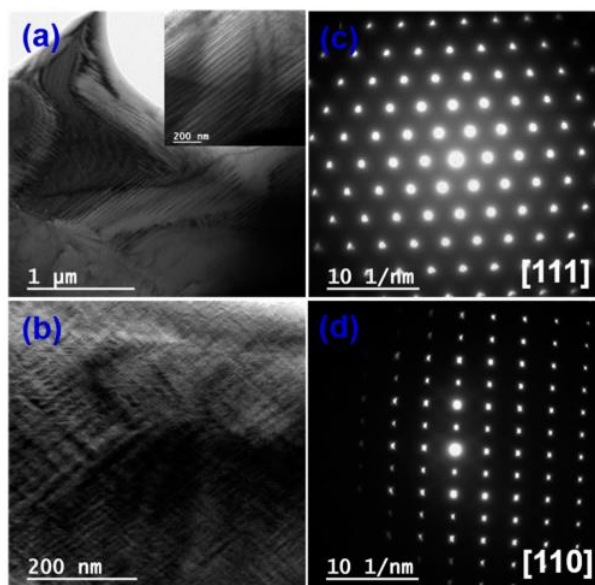
Fig 1.14 (a, b) Bright-field TEM images of domains structure of BCN at different magnification; the magnified view of thin domains is shown in the inset of (a). (c, d) SAED of the area is shown in the figure (a) and (b) [adopted from [55]]

In some older investigations, an excess CuO addition during synthesis and repeated heat treatment at elevated temperatures was shown to produce a well-resolved X-ray diffraction pattern of the compound with a tetragonal structure in the *P4mm* space group and lattice parameters 'a' = 4.046Å and 'c' = 4.180Å [54,56,57]. However, the extensive high-temperature treatment yielding a pure stoichiometric compound is somewhat debatable due to the low eutectic temperature of $CuO-Cu_2O$ (~1065°C) (Fig 1.15) [58] and the materials' decomposition as predicted by the observation of Ono et al. showing the formation of an oxygen-deficient compound [59].
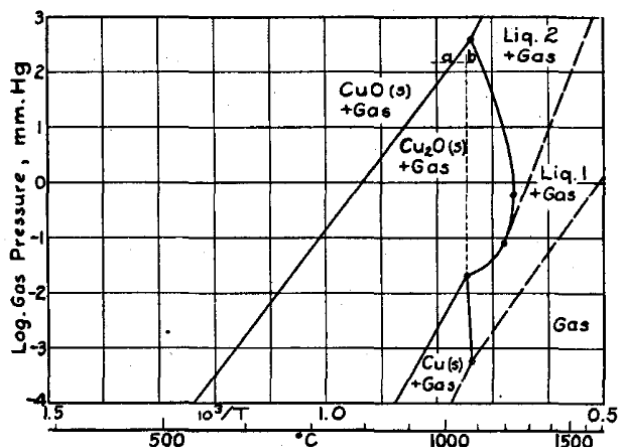
Fig 1.15 Pressure-temperature equilibrium phase diagram of Cu: Copper oxides [adopted from [58]]

The BCN compound has been explored as the end member of solid solutions with famous ferroelectric materials such as BNT, BT, BFO and PT. Less than four mol% of BCN has been studied along with BNT [60] and BT [61] in the form of solid solutions. The solubility limit of BFO with BCN was below 30 mol%, and the solid solution was also studied for multiferroic properties [62]. The solid solutions of BCN with all three, BNT, BFO and BT, possess an MPB within the mentioned composition range as shown in Fig 1.16, and their applicative properties are depicted in Fig 1.17((a-c) -BNT, (d and e) -BFO and (f and g) -BT). Only a few compositions (x = 0.90 and 0.95) of the solid solution $(1-x)Ba(Cu_{1/3}Nb_{2/3})O_3-(x)PbTiO_3$ [$(1-x)BCN-(x)PT$] have been investigated briefly for their dielectric and electromechanical properties by Priya et al. which are illustrated in Fig 1.17 (h and i)) [47].
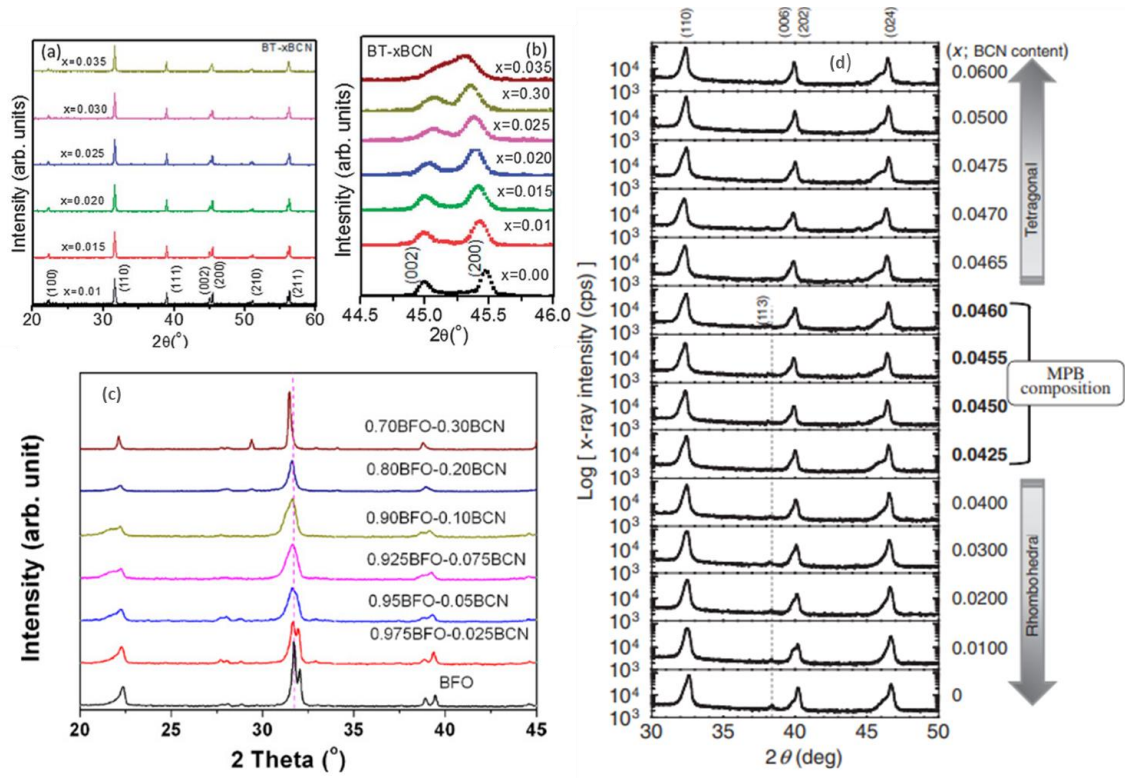
27

Fig 1.16 Composition dependent XRD pattern of (a, b) BT-xBCN, (c) BFO-xBCN and (d) BNT-xBCN [adopted from [60–62]]
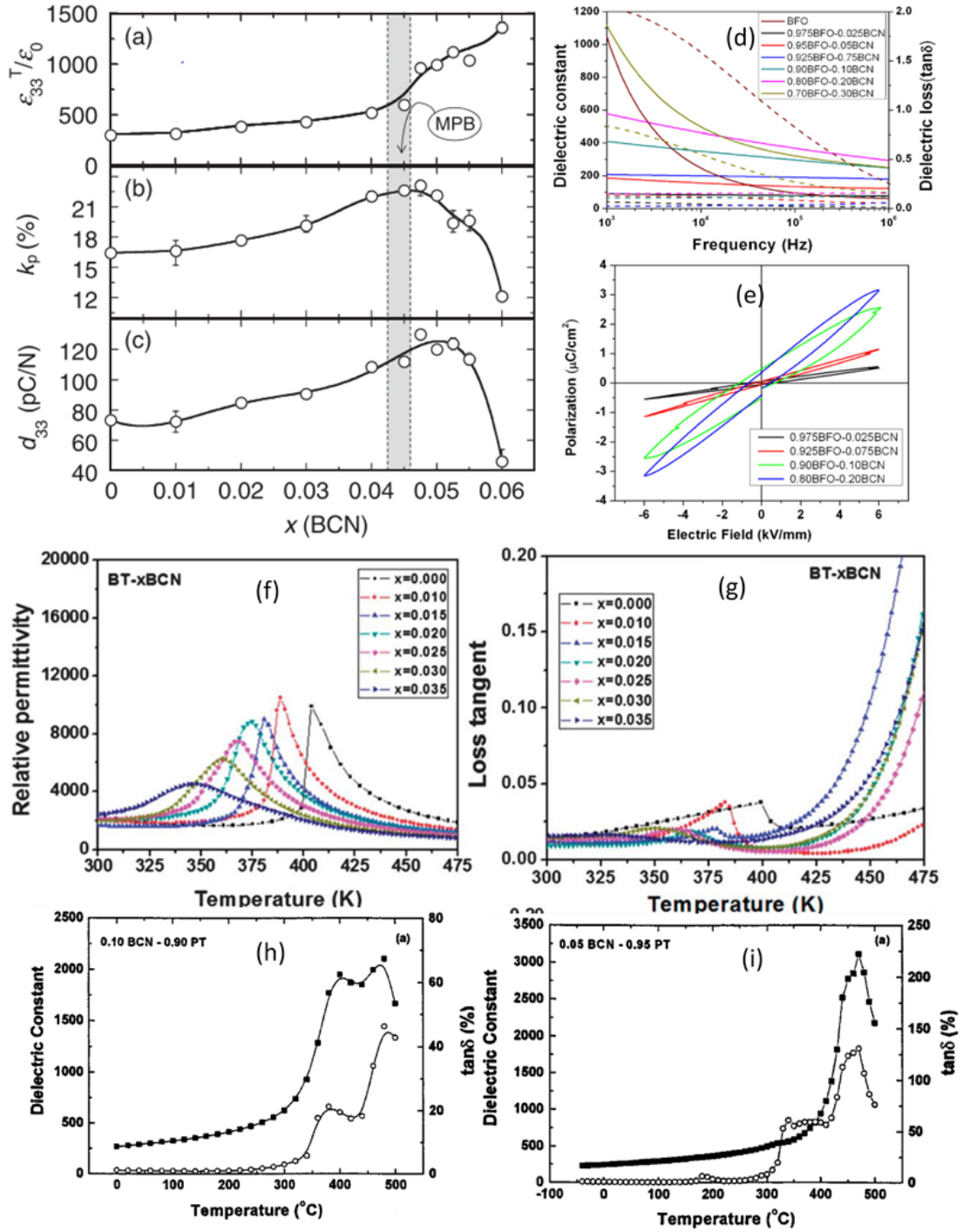
Fig 1.17 (a) $\varepsilon/\varepsilon_0$, (b) k_p, (c) d_{33} variation with concentration of BNT-xBCN; (d) frequency dependent dielectric constant; (e) P-E loop for different concentration of BFO-xBCN; (f) dielectric constant, (g) loss tangent for different concentration of BT-xBCN; dielectric constant and loss tangent for (h) (0.10)BCN-(0.90)PT and (i) (0.05)BCN-(0.95)PT [adopted from [47,60–62]]

1.14 Investigation of similar Solid Solutions with formulae (1-x) Ba(B'$_{1/3}$Nb$_{2/3}$)O$_3$-(x)PbTiO$_3$; B' = Mg, Zn, Yb, Lu, Sc

Some similar new PT-based solid solutions such as (1-x)Ba(Mg$_{1/3}$Nb$_{2/3}$)O$_3$-xPbTiO$_3$ (BMN-PT), (1-x)Ba(Zn$_{1/3}$Nb$_{2/3}$)O$_3$-xPbTiO$_3$ (BZN-PT), (1-x)Ba(Yb$_{1/2}$Nb$_{1/2}$)O$_3$-xPbTiO$_3$ (BYN-PT), (1-x)Ba(Lu$_{1/2}$Nb$_{1/2}$)O$_3$-xPbTiO$_3$ (BLN-PT), (1-x)Ba(Sc$_{1/2}$Nb$_{1/2}$)O$_3$-xPbTiO$_3$ (BSN-PT), (1-x)BaSnO$_3$-xPbTiO$_3$ etc., were explored a while ago [63–68]. Most of these systems possess an MPB with a rhombohedral-tetragonal type phase boundary existing between $0.71 \le x \le 0.74$, $0.65 \le x \le 0.70$, $0.58 \le x \le 0.61$, $0.64 \le x \le 0.68$ and $0.61 \le x \le 0.65$ composition range for BMN-PT, BYN-PT, BZN-PT and BLN-PT ceramics, respectively, as shown in Fig 1.18. These solid solutions possess d$_{33}$ in the range of 100~150pC/N and P$_r$ in the range of 10~18μC/cm^2, while T$_c$ varies around 55~250°C.
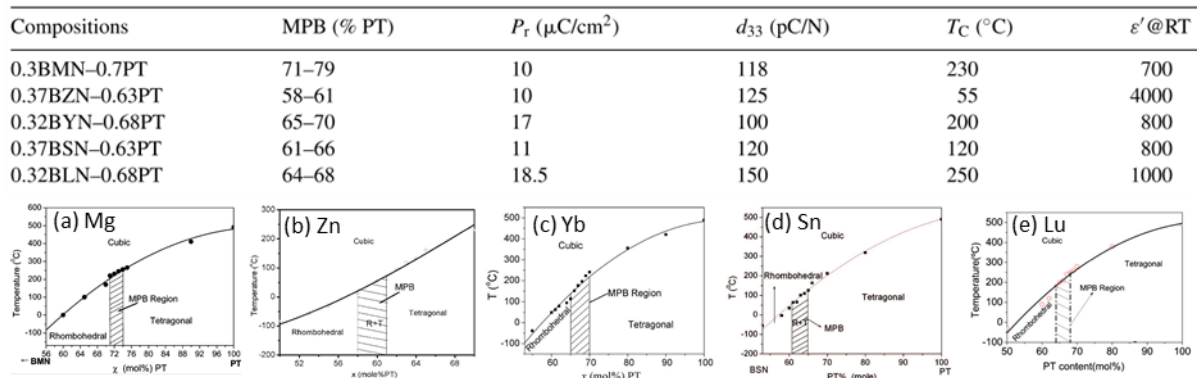
Compositions	MPB (% PT)	P_r (μC/cm^2)	d_{33} (pC/N)	T_C (°C)	ε'@RT
0.3BMN–0.7PT	71–79	10	118	230	700
0.37BZN–0.63PT	58–61	10	125	55	4000
0.32BYN–0.68PT	65–70	17	100	200	800
0.37BSN–0.63PT	61–66	11	120	120	800
0.32BLN–0.68PT	64–68	18.5	150	250	1000

Fig 1.18 Tabular illustration of properties (upper panel) and phase diagrams (lower panel) of (1-x) Ba(B'$_{1/3}$Nb$_{2/3}$)O$_3$-(x)PbTiO$_3$ piezoelectric ceramics; B' = (a) Mg, (b) Zn, (c) Sn, (d) Yb and (e) Lu [adopted from [52-57]]

1.15 Objectives of the Thesis

The ceramic solid solution (1-x)BCN-(x)PT has not been investigated yet for its crystal structure, microstructure, piezoelectric and ferroelectric properties in entire compositional span. Based on the literature review presented in the preceding sections, we selected this solid solution system for investigation in the present thesis. The objectives of the research were to develop a new low-cost, low-toxicity, flexible crystal-structured highly functional perovskite ceramic for various applications and investigate its crystal structure, dielectric, ferroelectric, piezoelectric properties as a function of composition and temperature. The specific objectives of the thesis are as follows:

1. Synthesis of different compositions at close interval of the new ceramic solid solution (1-x)BCN-(x)PT and optimization of calcination and sintering conditions.

2. Determination of crystal structure for all distinct phases within close compositional intervals of the solid solution with precision.

3. Investigation of the crystal structure of different compositions near MPB at temperatures ranging from cryogenic temperatures down to 15K, to high temperatures of 1073K.

4. Construction of a temperature vs. composition phase diagram for this solid solution.

5. Investigations of the microstructural, dielectric, ferroelectric and piezoelectric properties of solid solution.

6. Finding ways to improve the applicative characteristics of the solid solution with the lowest possible Pb content.

The subsequent chapters present the results of our investigations on (1-x)BCN-(x)PT ceramic and discussions on our new findings.